3D Atomic Imaging by Internal-Detector Electron Holography

Akio Uesaka,[1,2] Kouichi Hayashi,[3,*] Tomohiro Matsushita,[4] and Shigetoshi Arai[2]

[1]*Tohoku Techno Arch Company, Limited, Sendai 980-8577, Japan*
[2]*HORIBA Limited, Kyoto, 601-8510, Japan*
[3]*Institute for Materials Research, Tohoku University, Sendai 980-8577, Japan*
[4]*SPring-8/JASRI, Hyogo 679-5198, Japan*

(Received 19 May 2011; published 19 July 2011)

A method of internal-detector electron holography is the time-reversed version of photoelectron holography. Using an energy-dispersive x-ray detector, an electron gun, and a computer-controllable sample stage, we measured a multiple-energy hologram of the atomic arrangement around the Ti atom in $SrTiO_3$ by recording the characteristic Ti $K\alpha$ x-ray spectra for different electron beam angles and wavelengths. A real-space image was obtained by using a fitting-based reconstruction algorithm. 3D atomic images of the elements Sr, Ti, and O in $SrTiO_3$ were clearly visualized. The present work reveals that internal-detector electron holography has great potential for reproducing 3D atomic arrangements, even for light elements.

DOI: 10.1103/PhysRevLett.107.045502 PACS numbers: 61.05.js, 61.05.jp, 68.37.Hk

To develop state-of-the-art materials, knowledge of three-dimensional (3D) arrangements of atoms is important to understand the relationships between their physical properties and their structures. Atomic-resolution holography using electrons [1], x rays [2], or neutrons [3] can provide 3D images of atoms around specific elements without prior knowledge of their structures. Because of their elemental selectivities, atomic-resolution holography is especially powerful for determining the local structures around impurities, dopants, and adsorbates. Often, material physical properties are determined by them rather than by the matrix. In addition to this ability, another characteristic of atomic-resolution holography is a middle-range local structure analysis within 2 nm [4,5]. The x-ray absorption fine structure technique and the electron energy-loss fine structure technique can also investigate local atomic structures around a specific element; this can be adopted even for disordered materials. However, one can obtain only one-dimensional information about atomic distances, i.e., directionally averaged pair distribution functions. Moreover, the information obtained is usually limited to the second or third neighboring atoms due to the short mean free path of x-ray-excited photoelectrons.

Thus, atomic-resolution holography is more informative for local structure analyses. Holography, which was developed by Gabor [6] in 1948, can record the intensities and phases of waves scattered from an object, which are then used to reconstruct 3D images of that object. Szöke [7] proposed that atomic-resolution holography can be achieved by measuring the interference of photoelectrons or fluorescent x rays from samples. To date, atomic-resolution holography techniques with electrons [1,8], x rays [2,4,5,9], γ rays [10], and neutrons [3,11] have been developed and applied toward examining the environments around adsorbates [12], the local structures of dopants [13], quasicrystal structures [14], lattice distortions of mixed crystals [5], and the phase transition of a shape memory alloy [4]. However, since atomic-resolution holography has mainly been implemented in large experimental facilities, such as synchrotron radiation facilities or reactors, due to the need for energy-tunable and strong x-ray or neutron sources, its use has been limited, despite its great potential. We propose a method of internal-detector electron holography [15–17], which is the time-reversed version [9] of conventional photoelectron holography and uses electron beams as holographic waves and excitation sources. In contrast to x-ray or neutron beams, strong electron beams at the desired energies can be easily obtained at the laboratory scale. In this Letter, we demonstrate the recording of a multiple-energy hologram of the environment around Ti in $SrTiO_3$ using the internal-detector electron holography and the reconstruction of a real-space image using a fitting-based reconstruction algorithm.

Figures 1(a) and 1(b) show the principles of photoelectron holography and internal-detector electron holography, respectively. In photoelectron holography, part of a photoelectron wave from a source atom excited by x rays is scattered by neighboring atoms; it then interferes with the nonscattered photoelectron wave, forming an intensity distribution of photoelectrons outside the sample. The scattered and nonscattered electrons serve as the object and reference waves in the hologram, respectively. The intensity distribution of these photoelectrons can be interpreted as a hologram recording the atomic arrangement around atoms emitting photoelectrons. Atomic-resolution holography using wave sources inside samples, such as photoelectron holography, is called internal-source holography. By applying a Fourier transformationlike algorithm [18] to the hologram, a 3D atomic image can be obtained.

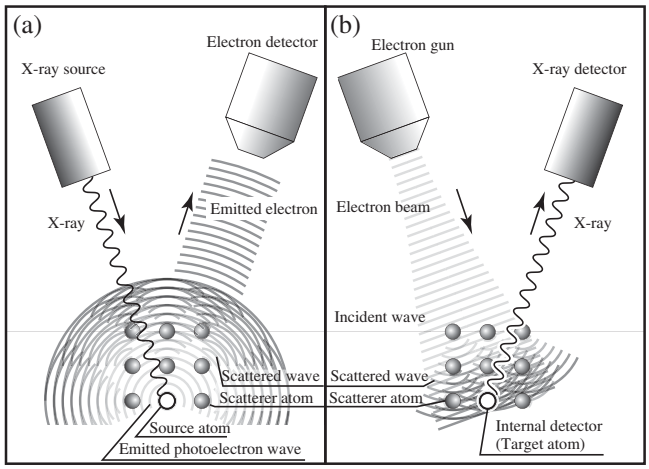

FIG. 1. Charts showing the principles of two schemes of atomic-resolution electron holography: (a) photoelectron holography and (b) internal-detector electron holography.

On the other hand, in internal-detector electron holography, an external electron beam is used for the generation of waves for holography and for the excitation of atoms. Part of the electron wave from the external source is scattered by neighboring atoms; it interferes with the nonscattered electron wave, resulting in the generation of an electron standing wave field pattern inside a sample. The intensity of characteristic x rays is proportional to the intensity of the electron wave field at atoms emitting characteristic x rays (target atoms), and it is modulated by the wave-number vector of the electron beam $\mathbf{k}$, whose holographic amplitude is approximated as

$$\chi(\mathbf{k}) = \sum_h [|\Psi_{\mathbf{a}_h}(\mathbf{k})|^2 + \Phi_0^*(\mathbf{k})\Psi_{\mathbf{a}_h}(\mathbf{k}) + \Phi_0(\mathbf{k})\Psi_{\mathbf{a}_h}^*(\mathbf{k})], \tag{1}$$

where $\Phi_0(k)$ and $\Psi_{\mathbf{a}}(k)$ are the reference wave function and the object wave function scattered by an atom located at $\mathbf{a}_h$, respectively, and h is the integer index for the atom. The target atoms act as monitors or detectors for recording holograms. The holograms have essentially the same structural information as is obtained by photoelectron holography.

Compared with conventional atomic-resolution holography techniques, the present method has a great advantage in terms of the ease of performing multiple-energy holography. Multiple-energy x-ray or photoelectron holography, which measures holograms at different energies (wavelengths), can strongly suppress false images and ghosts. Therefore, most x-ray holography experiments have been carried out by the multiple-energy method. However, multiple-energy holography requires an energy-tunable x-ray source such as synchrotron radiation. On the other hand, internal-detector electron holography uses an electron gun instead of an x-ray source. Since the acceleration voltage of the electron beam can be freely tuned, holograms at different electron wavelengths can be easily recorded in in-house experiments.

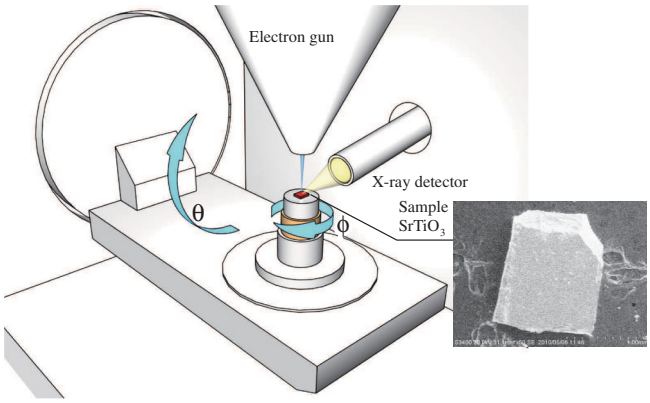

FIG. 2 (color). Experimental setup for internal-detector electron holography inside a SEM (Hitachi High-Technologies Corporation S-3400N). A Ge solid-state detector (CANBERRA GUL0055P) with a detection area of 50 mm^2 and a fast digital signal processor (XIA LLC DXP Saturn) were used to measure the Ti K line spectra. The θ-ϕ two-axis rotation stage was computer-controlled. The ϕ stage was continuously scanned during the recording of the hologram for each rotation of ϕ, and θ was increased in increments of 1.0°. The solid angle of the detector was 0.564 sr, and the emission current of the electron gun was 0.003 75 mA.

Figure 2 shows a schematic illustration of the experimental setup, which is composed of an electron gun, an energy-dispersive x-ray detector, and a sample stage that can change the incident angles of the electron beam. Because of the simplicity of the experimental setup, many similar experiments have been carried out in the past. For example, half a century ago, the interference of an incident electron beam was observed in the measurement of secondary electron emission with a change in the crystal sample orientation [19]. However, a clear hologram pattern, which can produce high quality atomic image, has not been reported because one must choose carefully the incident electron energy and estimate accurately the intensities of secondary radiation.

We used a single crystal of $SrTiO_3$ (001) to estimate the performance of the internal-detector electron holography method. Characteristic Ti $K\alpha$ x rays were excited by using 6.00–6.30 keV electron beams. We chose these electron acceleration voltages because they are close to the Ti K absorption threshold (4.965 keV). This effectively suppresses the Ti K lines caused by inelastically scattered electrons, which are incoherent and thus do not contribute to the formation of the hologram. Therefore, the use of an electron beam energy slightly higher than the absorption threshold is the key [16].

To perform multiple-energy holography, the electron acceleration voltages were chosen to be 6.00, 6.08, 6.15, 6.22, and 6.30 kV, with corresponding wave numbers k of 39.68, 39.95, 40.18, 40.41, and 40.66 $Å^{-1}$, respectively.

To minimize the twin image problem in multiple-energy holography for clear reconstruction, the adequate Δka range was estimated to be π, where a is the interatomic distance between the target and the scattered atoms [20]. In our experiment, since Δk is 9.8, $\Delta ka = \pi$ is satisfied at $a = 3.2$ Å. Thus, images of the first, second, and third neighboring atoms can be properly visualized by reconstruction from multiple-energy holograms recorded at these energies.

The sample stage of the scanning electron micrograph (SEM) was scanned two-dimensionally within the angular ranges of $0° \leq \phi \leq 360°$ ($\Delta\phi = 1.1°$) and $0° \leq \theta \leq 75°$ ($\Delta\theta = 1.0°$) while irradiating the electron beam, and the x-ray spectrum was detected at each point. The total number of spectra collected was 24 600. All of the intensities of the characteristic Ti $K\alpha$ x rays were estimated by applying the Gaussian fitting method to the spectra. The average intensity at each pixel is 4145 counts.

The obtained hologram is shown in Fig. 3(a). An approximately 10% undulation pattern was observed. We can clearly see forward-focusing peaks and dark lines. The dark lines are similar to Kikuchi lines in the photoelectron hologram. Here, we call them electron standing wave lines, analogous to the x-ray standing wave lines in inverse x-ray fluorescence holography. The intensities of the forward-focusing peaks are weaker than those of the normal holograms observed at 400–1000 eV photoelectron ranges.

To verify this measured hologram pattern, theoretical holograms of $SrTiO_3$ were calculated by using a 5457 atom cluster with a radius of 25 Å [21]. This calculated hologram pattern in Fig. 3(b) resembles the experimental

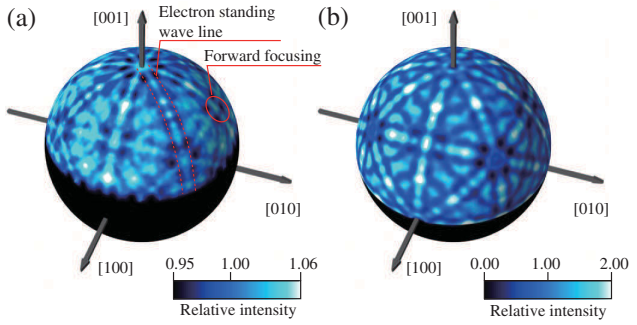

FIG. 3 (color). Holograms of $SrTiO_3$. (a) Experimental and (b) calculated holograms in **k** space. The acceleration voltage of the electron beam is 6.0 kV ($k = 396.8$ nm). In the hologram calculation, a spherical 5457 atom cluster with a radius of 25 Å was used. In both holograms, forward-focusing peaks and electron standing wave lines can be observed. The angular ranges of θ for the experimental and calculated data are $0° \leq \theta \leq 75°$ and $0° \leq \theta \leq 90°$, respectively. The intensities of both holograms were normalized with respect to their average intensities. The background intensity due to the excitation of Ti by inelastically scattered electrons was not taken into account in the calculation. Thus, the contrast of the hologram in (b) is much greater than that in (a).

pattern and reproduces the weak forward-focusing peaks and the electron standing wave lines. We found that the weak forward-focusing peak is a result of the long mean free path of the high-energy electron. It is known that a single scattering atom plays the role of an electron convex lens and produces a forward-focusing peak. However, when the mean free path is long, the electron must go through many scattering atoms in a line; i.e., the electron goes through many convex lenses. Therefore, the forward-focusing peak is defocused. The evident difference between the two patterns is in the contrast with the background. The reason for the low contrast of the experimental hologram originates from the characteristic x rays excited by inelastically scattered electrons, which were emitted mainly from deep regions. If we choose a very thin film with a thickness below the inelastic mean free path of the electrons (8 nm), the contrast will be improved by increasing the ratio of the characteristic x rays contributing to the hologram in the total ones.

The simplest and most commonly used tool for 3D atomic image reconstruction for atomic-resolution holography is the Barton algorithm [18], which is based on a Fourier transformation. However, in the case of internal-detector electron holography, this algorithm gives a blurred image because of the phase shift effect [22]. To overcome this problem, we adopted an advanced reconstruction method called the scattering pattern extraction algorithm using the maximum-entropy method (SPEA-MEM), which is a fitting-based reconstruction algorithm [23]. Because this algorithm, originally developed for photoelectron holography, includes phase shifts and angular anisotropies in electron scattering, it can reproduce a clear 3D image of the original atomic arrangement without artifacts or ghosts.

The theory of the SPEA-MEM is briefly explained here. Equation (1) can be extended as

$$\chi(\mathbf{k}) = \int G(\mathbf{a}) t(\mathbf{k}, \mathbf{a}) d\mathbf{a}, \tag{2}$$

$$t(\mathbf{k}, \mathbf{a}) = |\mathbf{a}|[|\Psi_{\mathbf{a}}(\mathbf{k})|^2 + \Phi_0^*(\mathbf{k})\Psi_{\mathbf{a}}(\mathbf{k}) + \Phi_0(\mathbf{k})\Psi_{\mathbf{a}}^*(\mathbf{k})], \tag{3}$$

where $t(\mathbf{k}, \mathbf{a})$ is defined as the scattering pattern function representing the holographic pattern produced by an atom located at position vector **a**. The function $|\mathbf{a}|G(\mathbf{a})$ represents the atomic distribution function. The maximum-entropy method is an effective method for obtaining the function $G(\mathbf{a})$. Before applying the SPEA-MEM, we extended the measured hologram data to a 4π sphere by using the crystal symmetry of cubic perovskite structures and the measured electron standing wave lines. Scattering patterns, as functions of the scattering angle and the distance from the scatterer, were obtained by calculating electron scattering by Ti atoms at 6.00, 6.08, 6.15, 6.22, and 6.30 keV. In this calculation, the multiple-scattering effect was taken into account, which is strong in the forward-scattering case.

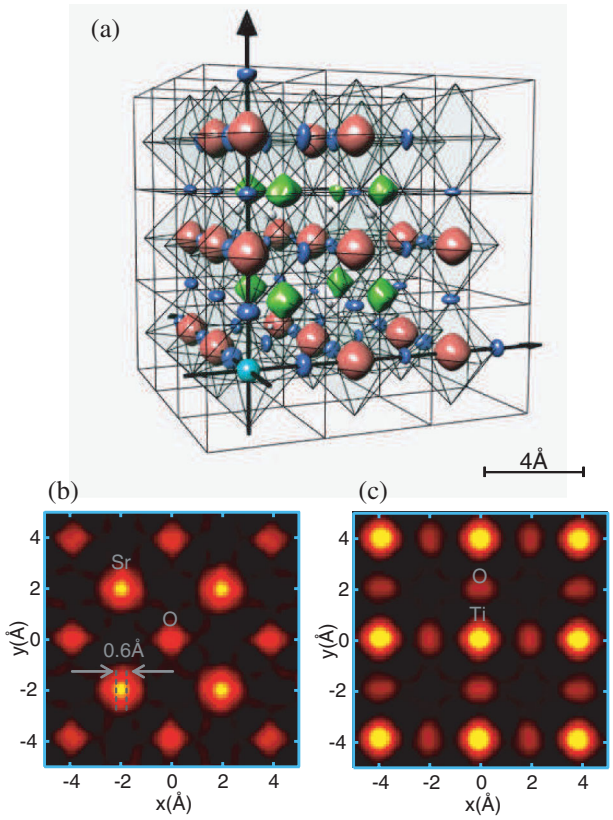

FIG. 4 (color). 3D images of $SrTiO_3$ reconstructed from multiple-energy holograms taken at 6.00, 6.08, 6.15, 6.22, and 6.30 kV. (a) Surface rendering of the reconstruction. Green, red, and blue objects correspond to Sr, Ti, and O atoms, respectively. Slices along the (001) plane at $z = 2$ (b) and 4 Å (c), which correspond to the Sr-O and Ti-O planes, respectively.

Figure 4(a) shows the 3D real-space images obtained around the Ti atom by using the SPEA-MEM. The atoms of all of the elements are clearly shown at the theoretical coordinates, even for the light element O, which is normally difficult to reconstruct due to its low-electron-scattering cross section. Generally, with increasing atomic weight, the image becomes more distinct. Two-dimensional images of the atoms in two crystallographic planes are shown in Figs. 4(b) and 4(c). In these figures, the images of heavier atoms are sharply reconstructed. The spatial resolution of the sharpest Sr images reaches 0.6 Å. Another interesting feature is the smearing of O images perpendicular to the Ti-O-Ti chains shown in Fig. 4(c). This smearing is due to the splitting of O atoms, resulting from the electronic instability of the Ti-O bonds [24]. Such smearing has also been observed in atomic images of O obtained by anomalous diffuse scattering [25].

In summary, using internal-detector electron holography, we successfully recorded multiple-energy electron holograms of $SrTiO_3$ at energies of approximately 6 keV. The measured holograms have the characteristic features of conventional photoelectron holograms, such as forward focusing and Kikuchi-line-like electron standing wave lines. Image reconstruction was also successfully implemented by using the SPEA-MEM, and it is sensitive even to the weak effect of the light atom smearing. Compared with conventional atomic-resolution holography techniques, the present method has a great advantage in its ease of performing multiple-energy holography, which can strongly suppress false images and ghosts. Moreover, since SEM has a spatial resolution on the order of micrometers, it will be possible to measure 3D atomic structures from micrometer-sized samples. In addition to the demonstration of the internal-detector electron holography, we have explored atomic-resolution electron holography at keV energies, the advantage of which is the capability of middle-range local structure analysis within the few-nanometer region owing to the long inelastic mean free path of keV electrons [26].

This work was supported by New Energy and Industrial Technology Development Organization (NEDO).

*khayashi@imr.tohoku.ac.jp

[1] G. R. Harp, D. K. Saldin, and B. P. Tonner, Phys. Rev. B **42**, 9199 (1990).
[2] M. Tegze and G. Faigel, Nature (London) **380**, 49 (1996).
[3] B. Sur *et al.*, Nature (London) **414**, 525 (2001).
[4] W. Hu *et al.*, Phys. Rev. B **80**, 060202(R) (2009).
[5] S. Hosokawa, N. Happo, and K. Hayashi, Phys. Rev. B **80**, 134123 (2009).
[6] D. Gabor, Nature (London) **161**, 777 (1948).
[7] A. Szöke, in *Short Wavelength Coherent Radiation: Generation and Applications*, edited by D. T. Attwood and J. Bokor, AIP Conf. Proc. No. 147 (AIP, New York, 1986), p. 361.
[8] J. Wider *et al.*, Phys. Rev. Lett. **86**, 2337 (2001).
[9] T. Gog *et al.*, Phys. Rev. Lett. **76**, 3132 (1996).
[10] P. Korecki, J. Korecki, and T. Slezak, Phys. Rev. Lett. **79**, 3518 (1997).
[11] L. Cser *et al.*, Phys. Rev. Lett. **89**, 175504 (2002).
[12] D. A. Luh, T. Miller, and T.-C. Chiang, Phys. Rev. Lett. **81**, 4160 (1998).
[13] K. Hayashi *et al.*, Phys. Rev. B **63**, 041201(R) (2001).
[14] S. Marchesini *et al.*, Phys. Rev. Lett. **85**, 4723 (2000).
[15] S. Y. Tong and H. Huang, Surf. Rev. Lett. **5**, 971 (1998).
[16] J. C. H. Spence and C. Koch, Phys. Rev. Lett. **86**, 5510 (2001).
[17] K. Hayashi, T. Matsushita, and E. Matsubara, J. Phys. Soc. Jpn. **75**, 053601 (2006).
[18] J. J. Barton, Phys. Rev. Lett. **67**, 3106 (1991).
[19] A. B. Laponsky and N. R. Whetten, Phys. Rev. Lett. **3**, 510 (1959).
[20] P. M. Len *et al.*, Phys. Rev. B **50**, 11 275 (1994).
[21] J. C. Slater, Phys. Rev. **81**, 385 (1951).
[22] P. M. Len *et al.*, Phys. Rev. B **59**, 5857 (1999).
[23] T. Matsushita *et al.*, Phys. Rev. B **78**, 144111 (2008).
[24] E. A. Zhurova and V. G. Tsirelson, Acta Crystallogr. Sect. B **58**, 567 (2002).
[25] M. Kopecký *et al.*, Phys. Rev. Lett. **100**, 195504 (2008).
[26] S. Thevuthasan *et al.*, Phys. Rev. Lett. **67**, 469 (1991).